Transitional DDES computations of the NREL Phase-VI rotor in axial flow conditions

Sørensen, Niels N.; Schreck, Scott

Published in:
Journal of Physics: Conference Series (Online)

Link to article, DOI:
10.1088/1742-6596/555/1/012096

Publication date:
2014

Document Version
Publisher's PDF, also known as Version of record

Transitional DDES computations of the NREL Phase-VI rotor in axial flow conditions

2014 J. Phys.: Conf. Ser. 555 012096

(http://iopscience.iop.org/1742-6596/555/1/012096)

Transitional DDES computations of the NREL Phase-VI rotor in axial flow conditions

Niels N. Sørensen and Scott Schreck

[1] DTU Wind Energy Division, Technical University of Denmark, Risø Campus, Bldg 115, Frederiksborgvej 399
[2] NREL's National Wind Technology Center, Golden, CO 80401, US.

E-mail: nsqr@dtu.dk

Abstract. In the present article we describe CFD simulations of the well known NREL Phase-VI rotor in axial flow conditions using a newly developed technique of combining turbulence modeling by the Delayed Detached Eddy Simulation (DDES) technique with laminar/turbulent transition modeling by a correlation based method. We demonstrate how the power production around the onset of stall is very dependent on the turbulence intensity in the inflow. Additionally, we compare with measurements and illustrate how the unsteady loads from the DDES simulations can provide valuable insight in the transient behavior of the rotor loads.

1. Introduction

The NREL Phase-VI rotor has been intensively studied since the first measurements were released in 2000 see the references of Fingersh et al. [1] and Simms et al. [2], and it has provided valuable insight into the aerodynamics of wind turbines, due to the high degree of details in these measurements, even down to time histories of the surface pressure. These data have played a strong role in the verification of CFD codes over the last more than 10 years, starting with the work of Sørensen [3, 4], Xu et al. [5], Duque et al. [6] and Benjanirat et al. [7]. Most of the studies have focused on the axial flow cases and has focused on time averaged loads, even though also the yaw cases have been investigated eg. early studies of Sørensen [3] and in the work of Madsen et al. [8]. In the present work the NREL Phase-VI experiment is used to validate unsteady loads during stall on the turbine operating in upwind configuration with axial flow.

2. Computational Method

2.1. Flow Solver

The in-house flow solver EllipSys3D is used in all computations presented in this paper. The code is developed in co-operation between the Department of Mechanical Engineering at the Technical University of Denmark and the former Department of Wind Energy at Risø National Laboratory, Risø-DTU, see [9, 10] and [11].

In the present work turbulence is modeled by the k-ω Shear Stress Transport (SST) eddy viscosity model [12] in the form of the Delayed Detached Eddy Simulation (DDES) technique of Menter and Kuntz [13], which is an extension of the DES model as proposed by Strelets [14]. The DDES methodology is combined with laminar/turbulent transition in the boundary layer on the blade which is modeled with the $\gamma - \widetilde{Re}_\theta$ correlation based transition model of Menter [15], for the present implementation see [16]. As the DDES methodology treats every thing except the separated region using the Reynolds Averaged Navier-Stokes (RANS) methodology, the transition model can be applied in the standard way within the boundary layer. The present work is extended

compared to the earlier computations of the Bertagnolio et al. [17], using higher grid resolution, DDES turbulence modeling and transition modeling.

The rotational motion is simulated by a moving mesh method, where the grid points in the computational mesh are all moved together as a solid body using a a general deforming mesh (DM) formulation in a fixed frame of reference. To assure that no artificial mass sources are generated by the mesh movement, the mesh velocities needed for the convective terms are computed enforcing the space conservation law, as described by [18].

The EllipSys3D code is second order accurate in time, using a second order backward differencing time discretization and sub-iteration within each time step. In the present computation, the diffusive terms are discretized with a second order central differencing scheme. The convective fluxes are computed using the QUICK scheme in the RANS regions while a fourth order central scheme is used for the regions where the DDES model has switched to Large Eddy Simulation (LES) technique.

The simulations are computed as transient runs with 1700 time-steps per revolution, and using 12 sub-iterations in each time-step. For the coarser grid levels only 850 time-steps are used per revolution.

The turbulence intensity at the rotor location is controlled by the specified inflow values of the turbulent kinetic energy k and the specific turbulence dissipation rate ω, along with the decay of the turbulence from the inlet to the rotor location. The decay can by estimated by the formula given by Langtry et al. [19], where t is the transport time computed from the free stream velocity and the distance from the inflow boundary to the rotor location:

$$k = k_{inlet}(1+\omega_{inlet}\beta t)^{-\frac{\beta^*}{\beta}} \text{ , with } \beta = 0.09 \text{ , and } \beta^* = 0.828 \text{ .}$$

2.2. Computational Grid

The mesh used for the present computations is based on an O-O topology. The surface mesh has 256 cells around the airfoils, 256 cells in the span-wise direction for each blade, and 256 cells in the wall normal direction. To facilitate the resolution of the tip of the blade, a 64×64 block is placed at each of the blade tips. The volume mesh is generated by the in-house HypGrid3D enhanced hyperbolic code. The y^+ values at the wall are kept below 2 everywhere on the blade surface. The mesh consists of a total of 136 blocks of 64^3 cells or a total of 36 million points. Wall boundary conditions in the form of no-slip boundary conditions are applied at the surface of the rotor blades. Inlet conditions in the form of Dirichlet conditions are specified over the part of the outer boundary shown in Figure 2, placed 10 rotor diameters from the rotor center. For the remaining part of the the outer boundary, the part of the outer surface not shown in Figure 2, outlet conditions are specified in the form of zero normal gradient conditions.

In contrast to typical RANS style computations, the grid resolution in the span-wise direction is highly increased to produce an area of nearly cubic cells in the vicinity of the rotor to allow optimal resolution of the small vortices near the rotor blades.

3. Results

The cases considered in the present work corresponds to the S-series from the Unsteady Aerodynamics Experiment Phase VI rotor from the National Renewable Energy Laboratory, see the report of Hand et al. [20]. The two-bladed 10.058 m diameter Phase VI rotor geometry is based on the S809 aerofoil, and details about the blades can be found in the report of Giguere and Selig [21]. For the cases considered in the present study, the rotor cone angle was set at 0°. The blade pitch angle was set at 3°, which rotated the blade tip chord-line 3° towards feather, relative to the rotor plane, pointing the leading edge into the oncoming wind. In this investigation, only the upwind configuration will be examined. In the present work wind speeds of 10, 12, 13, 15 and 20 m/s are considered. For all cases a rotational speed of 71.9 RPM and a density of 1.246 kg/m^3

Figure 1. The highly resolved surface of the rotor blades.

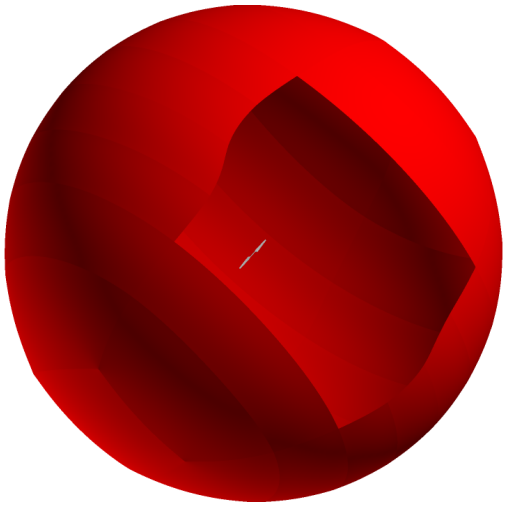

Figure 2. The computational domain, showing the rotor in the center of the domain and the inlet boundary in red.

and a viscosity of $1.769^{-5} kg/(ms)$ are used. Most cases are computed with an inflow turbulence intensity of 0.5% at the rotor location while a few additional computations are performed around stall to illustrate the high inflow dependency of the flow around stall. A qualitative picture of the wake predicted behind the rotor at 12 m/s by the present method can be seen in Figure 3, where the wake is visualized by the absolute value of the vorticity.

To quantify if the grid resolution is sufficient, the variation of the computed low speed shaft torque (LSST) for three different grid resolutions are investigated, using the grid sequencing capability of the Ellipsys3D code. The solution is initiated on a coarse version of the actual grid, constructed by successively removing every other point several times. In the present computations, three level of coarsening is used. The solution is initiated on level 3, where the fine grid have been coarsened two times and the number of cells is 64 times smaller than on the fine grid. Subsequent the solution is continued on level 2 where the number of grid points is 1/8 of the full grid, and finally the solution is finalized on level 1.

Looking at the low inflow turbulence cases the behavior of LSST as function of number of

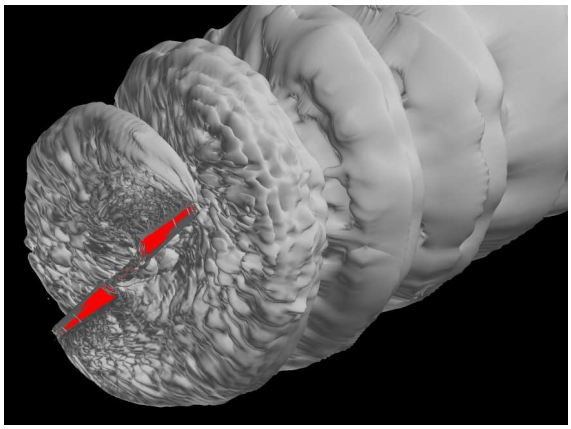

Figure 3. The turbulent wake behind the NREL Phase-VI turbine at 12 m/s, computed with the DDES model and transition.

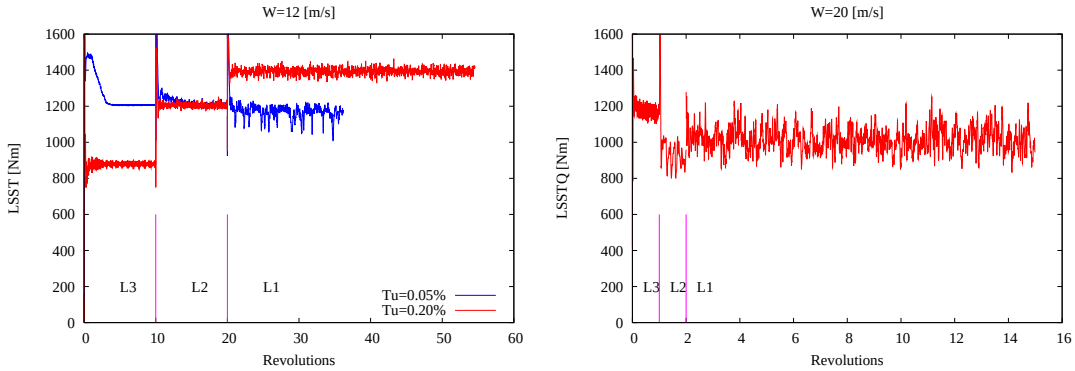

Figure 4. Time history for the Low Speed Shaft Torque at 12 and 20 m/s. The 12 m/s case show both a high and a low turbulent case. The vertical lines indicate the grid level shifts.

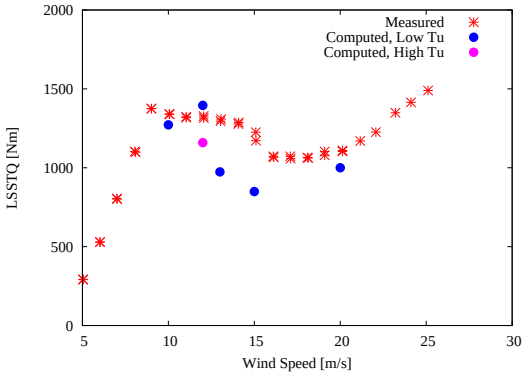

Figure 5. Comparison of measured and computed low speed shaft torque.

revolutions for the 12 and 20 m/s cases are shown in Figure 4. For the 12 m/s case where the transition location is very influential, the variation of the LSST with grid level is not negligible. From numerous 2D predictions, it has been shown that between 256 cells and 320 cells in chord-wise direction is sufficient to capture the right transition point location, but for the present level-2

grid with only 128 cells in chord-wise direction this criteria is not fulfilled, see the report of Sørensen [22]. In contrast, the high turbulent case where the transition point is placed close to the leading edge at 12 m/s exhibit much less grid dependency, see Figure 4.

For the 20 m/s case, level-3 is used between revolution 0 and 1, level-2 between revolution 1 and 2, while level-1 is used between revolution 2 and 15. For the 20 m/s case where the angle of attack is higher the transition point is again place close to the leading edge, and the grid dependency due to the transition model is again week. There is a clear shift in torque level between running on level-3 and level-2 while the change between level-2 and level-1 is minor. Based on these figures it is concluded that the grid resolution is sufficiently fine to give reasonable grid independent results, especially above 12 m/s where the major part of the unsteady shedding takes place.

The agreement of the predicted LSST to measured values is very similar to the agreement observed in earlier studies using RANS, e.g. the ones of Sørensen et al. [23]. In a previous study, it was shown that a strong dependency on inflow turbulence intensity of the LSST is observed using the transition model especially around stall, see Sørensen et. al. [16]. Here this behavior is reproduced with the DDES methodology only around the stall wind speed at 12 m/s, further investigations are not pursued due to the cost of the computations.

The conclusion from the present study is that the combination of the DDES methodology and transition modeling do not directly improve the prediction of the LSST or power production of the turbine, even though it comes at a considerable increase in mesh resolution and computational time.

Even though the new technique combining DDES and transition do not change the the quality of the mean power prediction, its value could for some application be its ability to predict the unsteady loads on the rotor, a thing that steady and unsteady RANS is not capable of. In order to show the difference between URANS and the DDES methodology, a single case of the present setup with unchanged grid and time-stepping was computed with URANS instead of DDES. As can be seen from Fig. 6, generally the energy content in the URANS is considerably lower than predicted by the DDES between a factor of 10 to nearly 100 especially at low frequencies. As seen in several previous studies URANS often produces very little unsteadiness even in separated flow, this can also be observed in the present study where the energy at high frequencies are often a factor of more than 10 lower than the DDES predictions.

The fact that even the DDES underestimate the energy contents, can be explained by two factors. First of all the lack of resolved turbulence in the inflow where the turbulence is not resolved but just modeled through the k-equation, this will results in a fully steady loading on the rotor blade for attached cases leading to underestimation of the spectra at low frequencies. Secondly, the finite resolution of the computational grid makes it impossible to resolve the very small turbulent eddies and is therefor responsible for some of the underestimation of the power spectra at high frequencies.

To illustrate the capabilities of the DDES we will look at the power spectral density of the thrust coefficients at several radial locations and for several wind speeds, and compare these to measurements, see Figure 6-9. For the lowest wind speed considered here, 10 m/s the flow is weakly stalled, and behaves very similar to a standard unsteady RANS prediction giving a steady solution without any significant time variations in the forces. Due to this the low wind speeds fails to give a meaning full power spectra, and no spectral results are shown.

For the 12 m/s case, the time history of the sectional forces start to exhibit unsteady behavior, see Figure 7, but no dominant shedding is observed in neither the computed or the measured frequency spectra. For the the 15 and 20 m/s cases, respectively the three and two innermost sections exhibit a clear vortex shedding frequency both in the measurements and in the computations. Besides the qualitative agreement, the predicted location of the frequency agrees well with the measured frequencies. Even though the frequencies are well predicted, there is due to the lack of resolved inflow turbulence and finite grid resolution some disagreement between the actual level of the power spectra, where the measured power spectra especially at higher

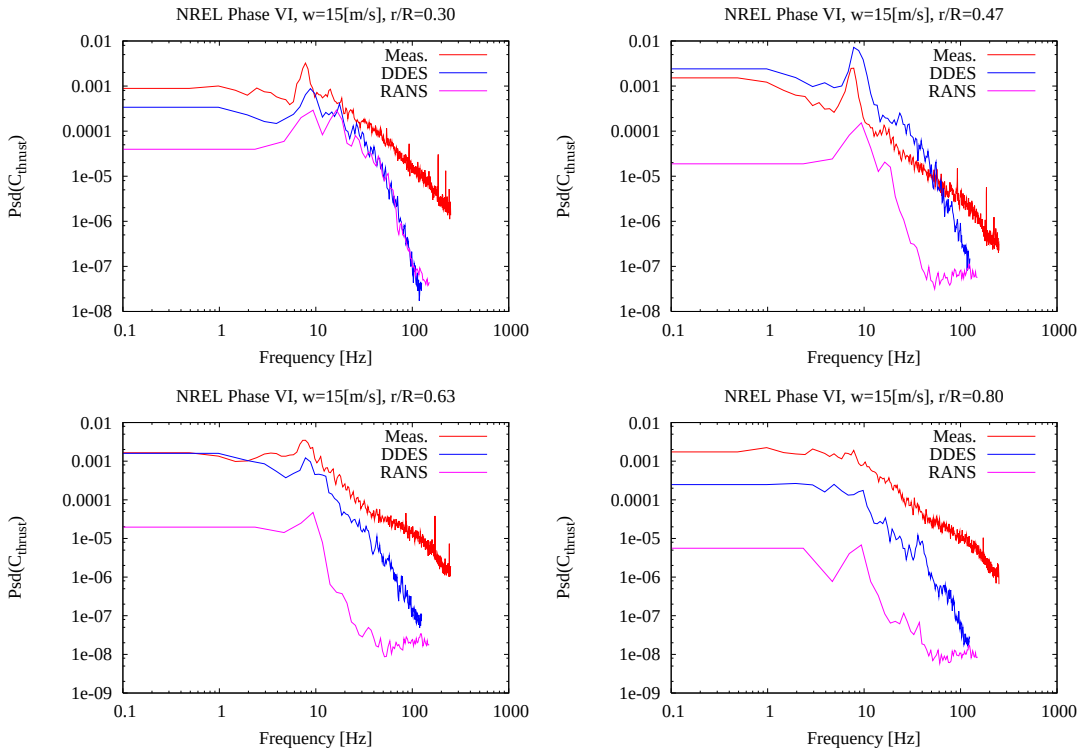

Figure 6. Comparison of URANS and DDES with measured and computed power spectral density computed from the thrust coefficient at several radial station for the 15 m/s wind speed case. From top left to bottom right, r/R= 0.30, 0.47, 0.63 and 0.80.

frequencies features higher energy.

Defining the Strouhal number for the vortex shedding as $St = c\sin\alpha f/U_{eff}$, where c is the airfoil chord length in meters, α for simplicity is taken as the geometrical angle of attack, and U_{eff} is the effective velocity seen by a given airfoil section in meters per second. The geometrical properties of the rotor can be seen from Table 1, while the U_{eff} and shedding frequency extracted from the power spectra can be seen from Tables 2 and 3. The expected behavior from early studies of flat plates at high angle of attack and bluff body flows is a Strouhal number around 0.15-0.18 based on the previous definition, see the work of Fage and Johansen [24] and the work of Roshko [25]. The Strouhal number at the most inboard station seems to fit well with these expectations, while a much lower value is observed at the outboard stations. Generally, the computed shedding frequencies shows good agreement with the observations as seen from the spectral plots and comparing with values extracted from Figure 6 in the work of Schreck [26]. The disagreement at the 0.63 radius for the 20 m/s situation is related to the sudden decrease observed experimentally when the wind speed increases from 19 to 20 m/s.

Looking at the shedding frequencies, it is observed that the frequency is approximately constant for the full blade span, see Table 2 and 3. As the inboard section Strouhal number behaves in accordance with expectations from non-rotating airfoil and bluff bodies, we speculate that due to the radial effects of the rotating system the outboard stations are forced to follow the frequency dictated by the inboard station instead of producing their natural Strouhal frequency.

This could be seen as both negative and a positive effect, as it may allow a simple control over the possible frequencies that will appear on the stalled rotor, while on the negative side the filtering property of the rotor is lost when all sections are stalling in phase.

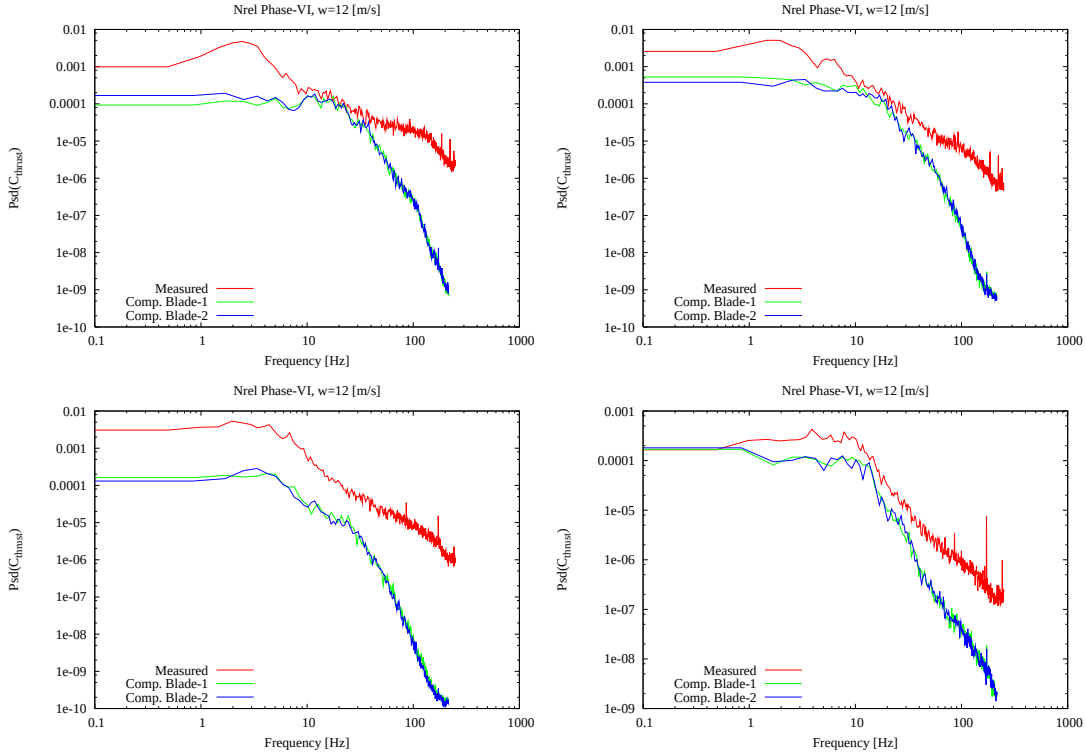

Figure 7. Comparison of measured and computed power spectral density computed from the thrust coefficient at several radial station for the 12 m/s wind speed case. From top left to bottom right, r/R= 0.30, 0.47, 0.63 and 0.80.

4. Conclusion

A series of zero yaw rotor computations are performed using a new methodology combining the Delayed Detached Eddy Simulation technique with laminar turbulent transition modeling.

It is discussed how the present methodology predict time averaged quantities e.g. the LSST with similar accuracy as the standard RANS approach for the present rotor. Similar to earlier findings using RANS, it is found that the LSST around the onset of stall is heavily influenced by the laminar turbulent transition process through the inflow turbulence intensity.

Due to the inherent unsteady nature of the present method it is well suited for predicting the vortex shedding frequency, and the predicted shedding frequencies show excellent comparison with the UAE Phase-VI experimental values. Due to lack of resolved inflow turbulence and the cut off at high frequencies due to limited grid resolution, the energy level is not well captured, but still severely improved compared to URANS type simulations. The present computations and the UAE Phase-VI experimental data indicate that the frequency of the vortex shedding for the full blade is dictated by the inboard sections and the overall three-dimensional flow field structure over the blade

Acknowledgments

The work was funded by the Danish Council for Strategic Research (DSF), under contract 2104-09-0026, Center for Computational Wind Turbine Aerodynamics and Atmospheric Turbulence. Computations were made possible by the use of the PC-cluster provided by DCSC and the DTU central computing facility.

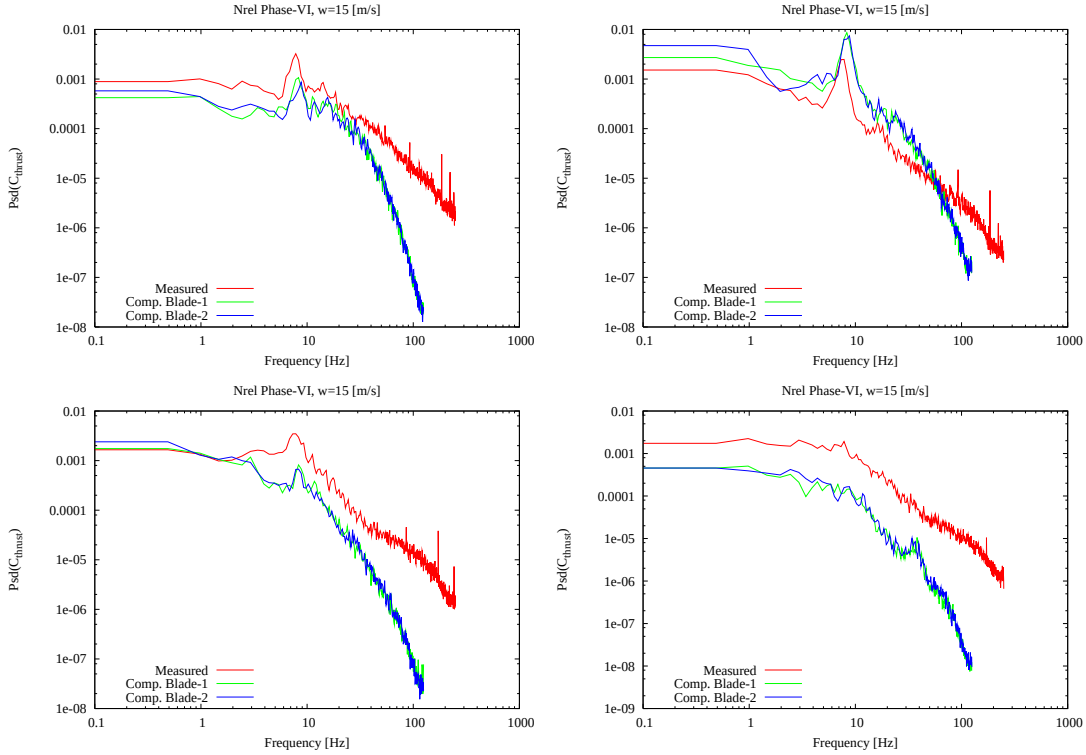

Figure 8. Comparison of measured and computed power spectral density computed from the thrust coefficient at several radial station for the 15 m/s wind speed case. From top left to bottom right, r/R= 0.30, 0.47, 0.63 and 0.80.

Table 1. Geometrical properties for the NREL Phase-VI rotor along the blade span, for the present cases the rotor blades are pitch 4.775 degrees toward feather.

Radius	Chord [m]	θ [deg]
0.30	0.71	14.31
0.47	0.62	4.59
0.63	0.59	1.16
0.80	0.46	-0.38
0.95	0.38	-1.47

Table 2. Strouhal numbers and shedding frequencies for the 15 m/s case.

Radius	U_{eff}	AOA [deg]	f [1/s]	St	St from [26]
0.30	18.8179	38.5454	7.81	0.18	0.18
0.47	23.2787	35.5281	7.44	0.12	0.12
0.63	28.1849	30.9943	7.56	0.08	0.07
0.80	33.8103	26.7172	7.80	0.05	0.04

References

[1] L. Fingersh, D. Simms, M. Hand, D. Jager, J. Cortrell, M. Robinsion, S. Schreck, and S. Larwood. Wind Tunnel Testing of NREL's Unsteady Aeordynamics Experiment. In *2001 ASME Wind Energy Symposium*, pages 129–135, Reno, NV, January 11-14 2001. ASME. AIAA-2001-0035.

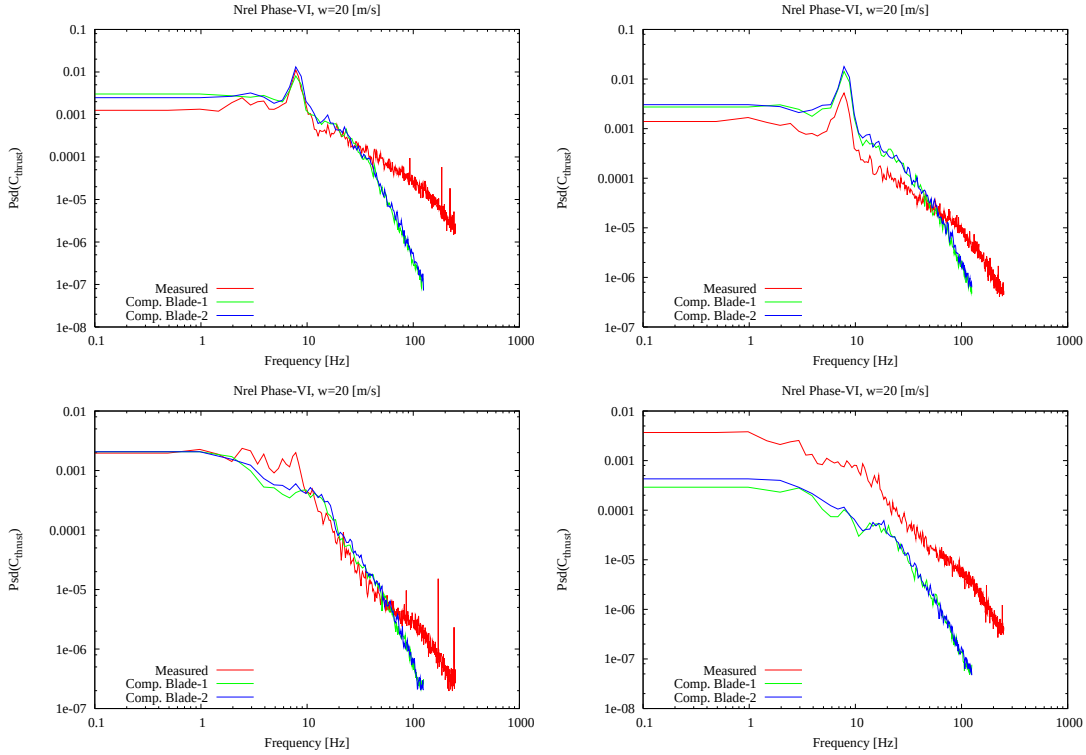

Figure 9. Comparison of measured and computed power spectral density computed from the thrust coefficient at several radial station for the 20 m/s wind speed case. From top left to bottom right, r/R= 0.30, 0.47, 0.63 and 0.80.

Table 3. W=20 [m/s]

Radius	U_{eff}	AOA [deg]	f [1/s]	St	St from [26]
0.30	23.0024	46.0874	7.81	0.17	0.18
0.47	26.775	43.7383	7.81	0.11	0.13
0.63	31.135	38.8084	7.80	0.07	0.00
0.80	36.3061	33.8068	2.88	0.02	0.00

[2] D. Simms, M. M. Hand, L. J. Fingersh, and D. W. Jager. Unsteady Aeorydnamics Experiment Phases II-IV: Test Configurations and Available Data Campaigns. NREL/TP -500-25950, Nat. Ren. Energy Lab., Golden, CO, 1999.
[3] N. N. Sørensen, J. A. Michelsen, and S. Schreck. Application of CFD to wind turbine aerodynamics. In Tsahalis D.T., editor, *CD-Rom proceedings. 4. GRACM congress on computational mechanics*, Patras, Greece, June 2002.
[4] N. N. Sørensen, J. A. Michelsen, and S. Schreck. Navier-Stokes Predictions of the NREL Phase VI Rotor in the NASA Ames 80 ft $\times$ 120 ft Wind Tunnel. *Wind Energy*, 5:151–169, 2002.
[5] G. Xu and Sankar. Application of a viscous flow methodology to the nrel phase vi rotor. In *ASME Conf. Proc., ASME 2002 Wind Energy Symposium*, 2002.
[6] Earl P.N. Duque, Michael D. Burklund, and Wayne Johnson. Navier-Stokes and comprehensive analysis performance predictions of the NREL phase VI experiment. *Journal of Solar Energy Engineering*, 125, Issue 4:457–467, 2003.
[7] Sarun Benjanirat, Lakshmi N. Sankar, and Guanpeng Xu. Evaluation of turbulence models for the prediction of wind turbine aerodytnamics. In *ASME 2003 Wind Energy Sysmposium*, 2003.
[8] Helge Aagard Madsen, Niels N. Sørensen, and Scott Schreck. Yaw aerodynamics analyzed with three codes in

comparison with experiment. In *ASME 2003 Wind Energy Symposium*, pages 94–103, Reno, Nevada, USA, January 6-9 2003.

[9] J. A. Michelsen. Basis3D - a Platform for Development of Multiblock PDE Solvers. Technical Report AFM 92-05, Technical University of Denmark, Department of Fluid Mechanics, Technical University of Denmark, December 1992.

[10] J. A. Michelsen. Block structured Multigrid solution of 2D and 3D elliptic PDE's. Technical Report AFM 94-06, Technical University of Denmark, Department of Fluid Mechanics, Technical University of Denmark, May 1994.

[11] N. N. Sørensen. General Purpose Flow Solver Applied to Flow over Hills. Risø-R- 827-(EN), Risø National Laboratory, Roskilde, Denmark, June 1995.

[12] F. R. Menter. Zonal Two Equation k-ω Turbulence Models for Aerodynamic Flows. *AIAA paper 1993-2906*, 1993.

[13] F.R. Menter and M. Kuntz. *The Aerodynamics of Heavy Vehicles: Trucks, Buses, and Trains*, volume 19 of *Lecture Notes in Applied and Computational Mechanics*, chapter Adaptation of Eddy-Viscosity Turbulence Models to Unsteady Separated Flow Behind Vehicles, pages 339–352. Springer, 2004.

[14] M. Strelets. Detached Eddy Simulation of Massively Separated Flows. AIAA Paper 2001-0879, Russian Scientific Center "Applied Chemistry" St. Petersburg, 2001.

[15] F. R. Menter, R. B. Langtry, S. R. Likki, Y. B. Suzen, P. G. Huang, and S. Völker. A Correlation-Based Transition Model Using Local Variables, Part I - Model Formulation. In *Proceedings of ASME Turbo Expo 2004, Power for Land, Sea, and Air*, Vienna, Austria, June 14-17 2004. ASME. GT2004-53452.

[16] Niels N. Sørensen. Cfd modelling of laminar-turbulent transition for airfoils and rotors using the $\gamma - \tilde{Re}_\theta$ model. *Wind Energy*, 12(8):715–733, 2009.

[17] Franck Bertagnolio, Flemming Rasmussen, Niels N. Srensen, Jeppe Johansen, and Helge Aagaard Madsen. A stochastic model for the simulation of wind turbine blades in static stall. *Wind Energy*, 13(4):323–338, 2010.

[18] J. H. Ferziger and M. Peric. *Computational Methods for Fluid Dynamics*. Springer-Verlag, 1996.

[19] R. B. Langtry, J. Gola, and F. R. Menter. Predicting 2D Airfoil and 3D Wind Turbine Rotor Performance using a Transition Model for General CFD Codes. AIAA-paper-2006-0395, 2006.

[20] M. Hand, D. Simms, L. J. Fingersh, D. Jager, S. Schreck J. Cotrell, and S. Larwood. Unsteady Aeorydnamics Experiment Phases VI: Wind tunnel Test Configurations and Available Data Campaigns. NREL/TP -500-29955, Nat. Ren. Energy Lab., Golden,CO, 2001.

[21] P. Giguere and M. S. Selig. Design of a Tapered and Twisted Blade for the NREL Combined Experiment Rotor. NREL/SR -500-26173, Nat. Ren. Energy Lab, Golden, CO, April 1999.

[22] Niels N. Sørensen. Airfoil computations using the - re model. Technical report, Ris National Laboratory for Sustainable Energy, Roskilde, 2009.

[23] N. N. Sørensen and J. A. Michelsen. Aerodynamic Predictions for the Unsteady Aerodynamics Experiment Phase-II Rotor at the National Renewable Energy Laboratory. AIAA Paper 2000-0037, 2000.

[24] F.C. Johansen A. Fage. On the flow of air behind an inclined flat plate of infinite span. In *Proc. Roy. Soc. A*, pages 170–197, 1927.

[25] A. Roshko. On drag and shedding frequency of two-dimensional bluff bodies. N.a.c.a. tn-3169, NACA, 1954.

[26] Scott Schreck. Low frequency shedding prompted by three-dimensionality under rotational augmentation. In *48th AIAA Aerospace Sciences Meeting*, AIAA Paper 2010-0640. American Institute of Aeronautics and Astronautics Inc., January 2010.